Macromolecules

pubs.acs.org/Macromolecules
Article

Confined Segmental Diffusion in Nanophase Separated Janus Polynorbornenes as Investigated by Quasielastic Neutron Scattering

Paulina Szymoniak, Mohamed A. Kolmangadi, Martin Böhning, Bernhard Frick, Markus Appel, Richard A. Mole, Nicolas R. De Souza, Reiner Zorn, and Andreas Schönhals*

Cite This: *Macromolecules* 2024, 57, 8562–8575
Read Online

ABSTRACT: A combination of neutron time-of-flight and neutron backscattering spectroscopy was used to investigate the molecular dynamics of Janus polynorbornenes (Janus poly(tricyclononenes)) on a microscopic level. These Janus polynorbornenes, denoted as PTCNSiOR, have a semirigid backbone with $-Si(OR)_3$ side groups attached to it. R represents the length of the alkyl side chain. Here side chain lengths of R = 3 (propyl) and R = 8 (octyl) were considered. It is worth mentioning that these polymers have some potential as active layers in gas separation membranes, especially for the separation of higher hydrocarbons. The combination of time-of-flight and backscattering will ensure a reasonably broad time window for analysis where the incoherent intermediate scattering function $S_{Inc}(q,t)$ is considered. Previously, it was shown by X-ray investigations that the system undergoes a nanophase separation into alkyl side chain-rich domains surrounded by a backbone-rich matrix. For PTCNSiOPr (R = 3), the alkyl side-chain-rich domains are truly isolated in the backbone-rich matrix, whereas for PTCNSiOOc (R = 8) these domains percolate through the matrix. Further, it was also previously shown that the alkyl side-chain-rich domains undergo a glass transition. The advantage of neutron scattering experiments discussed here is that besides temporal also spatial information is obtained which will allow conclusions to be drawn about the type of molecular fluctuations. At the lowest measured temperature, the decay in $S_{inc}(q,t)$ is due to the methyl group rotation. The methyl group dynamics is analyzed in terms of a modified jump-diffusion in a 3-fold potential and yields to a reasonable fraction of hydrogens which contribute to the methyl group rotation. At higher temperatures, the decay in $S_{Inc}(q,t)$ is due to both the methyl group rotation and the segmental dynamics in the alkyl side-chain-rich domains. The segmental diffusion is modeled by a sublinear diffusion. For the analysis of the scattering function $S_{Inc}(q,t)$ of PTCNSiOPr an elastic scattering due to the immobilized backbone-rich matrix must be taken into account. The analysis reveals that the segmental dynamics is confined by the finite size of alkyl chain-rich domains and that it is intrinsically heterogeneous in nature. Both effects are more pronounced for PTCNSiOPr in comparison to those of PTCNSiOOc.

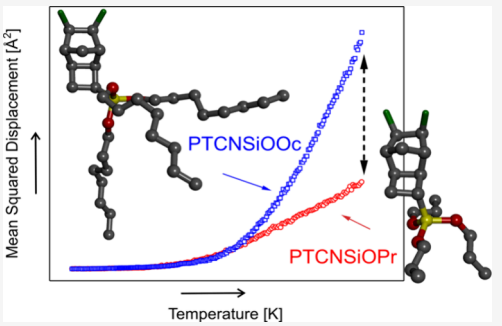

1. INTRODUCTION

Separation processes are central technologies in chemical and related industries such as energy supply. In the field of gas separation, conventional approaches use adsorption or cryogenic distillation, but these processes are costly and energy consuming. For a sustainable energy supply in the future, these classical technologies must be replaced by more cost- and energy-efficient processes such as membrane separation using polymers for the active separation layer. A further advantage of membrane processes is that they can be employed at large scales, such as for the purification of natural gas, as well as on smaller, local scales, like the upgrading of biogas or the separation of hydrogen and methane in urban gas distribution grids. For these applications the polymer for the separation layer must have high permeability (flux) and a good selectivity for a gas pair a,b.[1,2]

Glassy polymers make up the most promising class of materials for the active separation layer in membranes. For gas separation applications, the glassy polymer should have a high free volume. This high free volume content is motivated by the solution diffusion mechanism which is the widely accepted model for gas transport in dense polymers.[3] In this model, after a sorption of the gas molecules described by their solubility, S, diffuse through the polymer controlled by their diffusion coefficient, D. This diffusion process leads to a gradient in the concentration of the gas molecules. Individual jumps of gas molecules between free volume elements are considered a mechanism for diffusion. As the formation of temporary channels is required to allow for such jump events, the diffusive

Received: May 8, 2024
Revised: August 14, 2024
Accepted: August 16, 2024
Published: August 22, 2024

https://doi.org/10.1021/acs.macromol.4c01045
Macromolecules 2024, 57, 8562–8575

transport is related to the molecular mobility of the surrounding polymer. Therefore, it is important to investigate the molecular mobility for polymers that are suited for membrane applications besides the gas transport quantiles.

The perception that the gas transport in polymers is due to the fractional free volume and the molecular mobility leads to two different main directions for optimizing macromolecules for these purposes. The first direction is the development of new glassy polymers with extraordinarily high values of the fractional free volume such as poly(trimethylsilylpropyne) (PTMSP)[4] and poly(4-methyl-2-pentyne) (PMP).[5,6] These polyacetylenes have permeability values that are by orders of magnitude higher than that of polysulfones or other conventional glassy polymers. Unfortunately, the observed values of the selectivity for these polymers are insufficiently low due to the connected large pores. However, the quest for synthesizing polymers with a high free volume content leads to novel classes of polymers. One group of such novel macromolecules are polymers of intrinsic microporosity known as PIMs.[7−10] PIMs have large values of Brunauer−Emmett−Teller (BET) surface areas in the range of several hundred m^2/g. The microporosity is due to pores with characteristic sizes in the range of 0.5−2 nm forming an interconnected network.[11,12] The molecular origin of the microporosity of PIMs is due to rigid ladder-type backbones with a contorted structure induced, for example, by spiro-centers leading to an inefficient packing of segments when a condensed state is reached from the solution. Besides PIMs, a second class of microporous polymers has been developed which consist of addition polymerized polynorbornenes with a relatively stiff backbone and bulky side groups (see for instance refs 13−18). Examples of this kind of polymer are, for instance, Si-substituted poly(tricyclononenes). For this class of polymers, the inherent microporosity arises from a semistiff backbone with sterically demanding, bulky side groups. These side groups hinder conformational changes leading, like for PIMs, to insufficient chain packing during the solidification from a dilute solution. Because of their specific microporosity, PIMs and microporous polynorbornenes combine high permeabilities with reasonably high permselectivities. The origin of this selectivity is still poorly understood, as from the interconnected microporous network a less selective Knudsen-like diffusion is expected theoretically. Recently it was shown for a PIM that for small gas molecules (H_2, He) the diffusion is Knudsen-like whereas for larger gas molecules (O_2, N_2, CO_2, or CH_4) the diffusion obeys the solution diffusion model.[19] It is discussed that molecular fluctuations of the polymeric matrix can open or close bottlenecks between pores, which allow so for the selective gas transport. Also, for this purpose, the molecular mobility should be investigated.

The second main direction to optimize polymers for gas separation starts from the idea of tailoring the molecular mobility of polymers in the glassy state.[20−22] Recently, Alentiev et al. reported the preparation of a homologous series of Janus poly(tricyclononenes) by addition polymerization.[23] These Janus poly(tricyclononenes) have a rigid backbone of norbornene repeating units, where each repeating unit has three flexible alkyl side chains ($-Si(OR)_3$). The length of the alkyl chain was systematically varied in a larger range. From an applicational point of view, it is worth mentioning that these Janus polynorbornenes have a higher selectivity for the separation of longer hydrocarbons.[23] Utilizing broadband dielectric spectroscopy (BDS), temperature-modulated DSC (TMDSC), and fast scanning calorimetry (FSC) combined with X-ray scattering an in-depth investigation of these polymers was reported elsewhere.[24] By a quantitative analysis of the X-ray measurements, it was revealed that this polymer system is nanophase-separated, having alkyl side chain-rich and norbornene backbone-rich domains. The term "backbone-rich domains" just refers to a backbone-rich phase that is amorphous with long-range order or packing. This consideration is supported by the experimental result that a separate glass transition is observed by calorimetric measurements in ref 24. The characteristic size of the alkyl side chain-rich domains increases with the length of the side chain. For the polymer with the *n*-propyl side-chains the alkyl chain-rich domains are surrounded and isolated by a backbone-rich matrix. In difference for the polymer with *n*-octyl side-chains the alkyl chain-rich domains percolate through the matrix.[24] The latter conclusion was derived from the dependence of the conductivity on the size of the alkyl side chain-rich domains. Moreover, the dielectric and calorimetric data show that the alkyl chain-rich domains for both polymers undergo a glass transition. Because of the small size of the alkyl chain-rich domains, it can be considered as a hindered glass transition.[24,25]

The microscopic dynamics of high performance polymers like polyacetylenes was investigated by quasielastic neutron scattering (QENS).[26−28] By these experiments it was evidenced that the permeabilities for CO_2 or CH_4 can be related to molecular motions at a time scale of picoseconds at room temperature.[26,28] Kanaya et al. developed a so-called random gate model.[27] In the framework of this model, localized fluctuations enable the gas transport in polymers. This conclusion was further supported by a correlation of the activation energies of the permeation and localized fluctuations measured by dielectric spectroscopy.[29]

For PIMs and microporous polynorbornenes, no glass transition temperature was found by conventional scanning calorimetry before their thermal degrdation. Therefore, the glass transition behavior of these materials was investigated by fast scanning calorimetry which enables for heating rates up to 10^4 K/s.[30−32] For the archetypal PIM-1 a glass transition temperature of 644 K at a heating rate of 10^4 K/s[31] was found. For the Janus polynorbornene with the shortest alkyl side-chain (propyl) a glass transition temperature of the polynorbornene-rich matrix was found to be ca. 675 K at a heating rate of 5000 K/s.[24] In addition to calorimetric experiments the molecular mobility of bot PIM-1 and microporous polynorbornenes was also investigated by broadband dielectric spectroscopy to understand in part the physical aging in such systems.[33−36] Several dielectric active processes were observed for these high-performance polymers. It is worth mentioning that one of these processes was assigned to a kind of Maxwell−Wagner−Sillars polarization due to blocking of the charge carrier at the pore walls of the interconnected microporous network. The molecular mobility of high-performance polymers was further studied also by QENS experiments on PIM-1[37] and on microporous polynorbornenes.[38] As no glass transition was found for these polymers, in these investigations, the attention was focused on localized fluctuations like the methyl group dynamics. It was analyzed in terms of a jump diffusion in a 3-fold potential. When the correct number of hydrogens is taken into consideration, this approach describes the dependence of the elastic incoherent structure factor on the scattering vector correctly. Besides the

https://doi.org/10.1021/acs.macromol.4c01045
Macromolecules 2024, 57, 8562−8575

localized fluctuations of these high-performance polymers, the low-frequency density of states was studied by inelastic neutron scattering for PIM-1 and for several microporous polynorbornenes with different values of the BET surface area.[39,40] A correlation between the maximum frequency of the excess contribution to the Debye-like density of states and BET surface area was found, which evokes implications for applications as gas separation membranes.

In the present study, quasielastic neutron scattering is employed to investigate the microscopic dynamics of two Janus polynorbornenes with $-Si(OR)_3$ alkyl side chains where two different side chain lengths R = *n*-propyl and R = *n*-octyl are considered. An investigation of the low-frequency density of states of these Janus polynorbornenes was presented elsewhere.[41] The presented work is designed to investigate the molecular dynamics in a complex polymer system from a fundamental point of view. It is not aimed at contributing directly to membrane science. Work is in progress to establish a connection between gas transport data and the results of quasielastic neutron scattering.

2. MATERIALS AND METHODS

Materials. Two poly(tricyclononenes) (PTCN) with $-Si(OR)_3$ side chains are considered where the lengths of R are R = 3 (*n*-propyl, PTCNSiOPr) and R = 8 (*n*-octyl, PTCNSiOOc). It is worth mentioning that in both cases the alkyl side-chains are terminated by a methyl group. The general chemical structures of the repeating units of both polymers are depicted in Figure 1. The synthesis of the

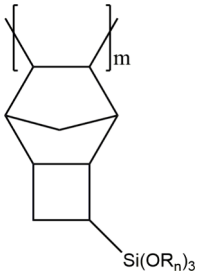

Figure 1. Chemical structure of the considered Janus polynorbornenes where R is the lengths of the alkyl side chains with n = 3 and 8.

polymers is described in refs 23 and 41 for PTCNSiOPr and in the Supporting Information of ref 24 for PTCNSiOOc. Table 1 gives the molecular weights of the considered polymers. For PTCNSiOPr a BET surface area of less than 10 m^2/g was found. For PTCNSIOOc no BET surface value could be measured. Therefore, it can be concluded that considered both Janus polynorbornenes are not microporous, compared to other high-performance polynorbornenes.[16]

Figure 2 gives the X-ray pattern for PTCNSiOPr and PTCNSiOOC in the SAXS–WAXS range.[24] The peak at the highest

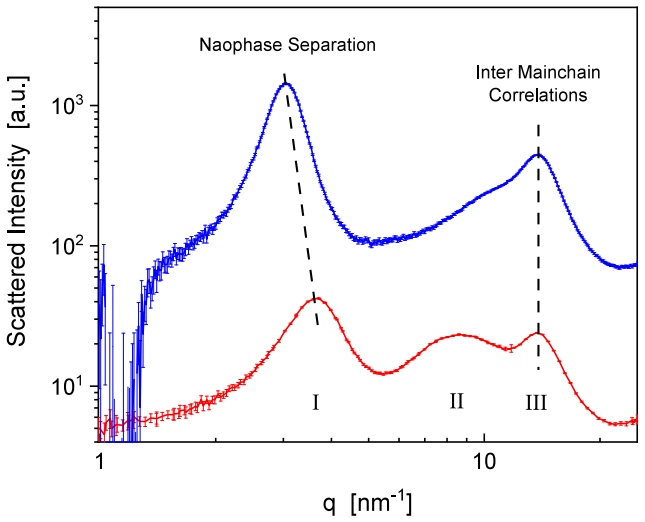

Figure 2. X-ray patterns for PTCNSiOPr (red) and PTCNSiOOc (blue). The data were taken from ref 24. For sake of clearness, the curves are shifted along the Y-axis.

Table 1. Molecular Weights of the Janus Polynorbornenes PTCNSiOPr and PTCNSiOOc Are Taken from Ref 24 and Sizes of the Nanophase Separated Alkyl Chain-Rich Domains Are Taken from Ref 24

	M_n [g/mol]	M_w [g/mol]	polydispersity	size of the domains [nm]
PTCNSiOPr	1.2×10^5	8.3×10^5	6.6	1.72
PTCNSiOOc	3.3×10^5	7.1×10^5	3.2	2.1

As no information about the shape of the of the alky chain-rich domains can be extracted from the X-ray pattern, this is the simples possible approach which has been also used for nanophase separated poly(*n*-alkyl methacrylates).[25,42] In a spatially periodic system, the Bragg equation gives a characteristic distance which is referred to here as characteristic size in agreement with ref 25.

q vectors is related to polynorbornenes backbone correlation as its position is not dependent on the length of the alkyl side chain. For instance, such short-range carbon–carbon correlation was also observed for simple liquids[43] but also for polythiophenes.[44] The one at intermediated q values is assigned to a hidden microporosity (no interconnected microporosity) in PTCNSiOPr. The peak observed at the lowest values of the q vector is related to the size of the microphase-separated domains of the alkyl side chains. For this assignment seen also ref 25. From the maximum position of that peak, the size of the alky side chain-rich domains is estimated by the Bragg equation (see Table 1). In the literature there is no consensus as to whether the morphology in polymers with long *n*-alkyl methacrylate side chains is quasi -1D (interdigitated) or spatial 3D.[25] In ref 24 it was found that characteristic size of the alkyl side chain-rich domains has a weaker dependence on the number of the carbon atoms in the side chain than expected for an all-trans conformation. This points rather to a 3D structure than to a 1D one. The X-ray pattern for both Janus polynorbornenes gives no evidence for a hexagonal ordered phase as discussed in ref 45 for brush copolymers. A hexagonally ordered structure inevitably creates a higher order reflection at $\sqrt{3}q_{max}$ where q_{max} is the position of the first reflection. Such a reflection is not observed in the X-ray pattern.

The sample preparation is given in detail in ref 24. In brief, PTCNSiOPr and PTCNSiOOc were dissolved in toluene. To minimize multiple scattering events, the thickness of the sample films should be adjusted to enable for ca. 10% neutron scattering. Therefore, the concentration of the solutions was adjusted for that purpose. A PTFE mold was used to cast the solution, which was filtered by a PVDF filter with pores of 0.2 μm. The sample form was placed in a closed chamber saturated with chloroform vapor to slow and control the initial evaporation of the solvent. The film, which was formed after 3 days, was moved to a vacuum oven with an oil-free vacuum to be annealed at 393 K for a further 3 days for complete solvent removal. The thicknesses of the samples were 0.146 mm for PTCNSiOPr (10% calculated scattering) and 0.102 mm for PTCNSiOOc (8.2% calculated scattering). As the final step, the films were placed in flat aluminum containers that were hermetically closed by electrowelding. These sample containers were used for the neutron experiments, as aluminum is nearly transparent for neutrons.

https://doi.org/10.1021/acs.macromol.4c01045
Macromolecules 2024, 57, 8562–8575

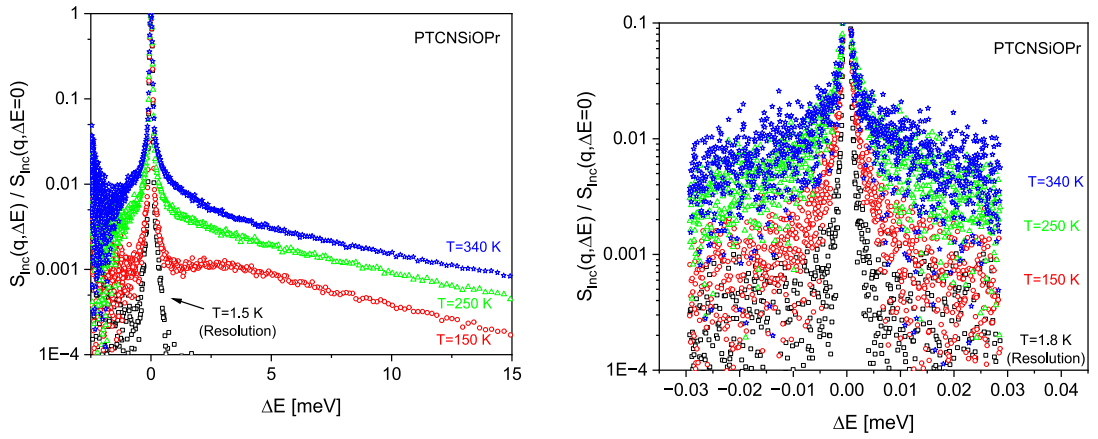

Figure 3. (a, left) Incoherent dynamical structure factor $S_{Inc}(q,\Delta E)$ divided by the height of the elastic line versus energy transfer ΔE for PTCNSiOPr for the indicated temperatures at a scattering angle of 89° (q = 1.62 Å^{-1}) measured at Pelican. (b, right) Incoherent dynamical structure factor $S_{Inc}(q,\Delta E)$ divided by the height of the elastic line versus energy transfer ΔE for PTCNSiOPr for the indicated temperatures at a scattering angle of 118° (q = 1.72 Å^{-1}) measured at IN16B.

Neutron Scattering. For the neutron scattering experiments, different modes have been used: elastic fixed windows scans (elastic scans) and quasi-elastic neutron scattering experiments.

Elastic Scans. Elastic scans on a neutron backscattering spectrometer ($\Delta E \approx 0$) provide an overview of the molecular dynamics on a time scale corresponding to the resolution of the instrument (0.8 μeV, ca. 2 ns). For these experiments the cold neutron backscattering spectrometer IN16B is used.[46−48] IN16B is hosted by the Institut Laue-Langevin (ILL) in Grenoble, France. It is a backscattering spectrometer of the third generation using focusing optics and employing a phase-space transformer to enhance the intensity as well as a linear-motor Doppler drive. A standard high flux configuration with unpolished Si-111 monochromators−analyzers was used for the measurements. The incident wavelength of the neutrons was 6.271 Å. The maximum value of the accessible elastic scattering vector is 1.9 Å^{-1}. For the elastic fixed windows scans, the Doppler drive is at rest. The elastic scattering at the lowest temperature was measured with a better statistic, as this value is used as reference for the analysis.

Quasielastic Neutron Scattering Experiments. By quasielastic neutron scattering, the scattering function $S(q,\Delta E)$ is measured in the dependence on the scattering vector q (momentum transfer) and the energy transfer ΔE. In the experiments, neutron time-of-flight scattering was combined with neutron backscattering to obtain a reasonably broad time range for the analysis.

The medium-resolution cold neutron spectrometer Pelican, operated at the Australian Nuclear and Technology Organization (ANSTO, Lucas Heights, Australia), was utilized as a time-of-flight (TOF) spectrometer.[49] Pelican uses a focusing crystal monochromator and two Fermi choppers to obtain a pulsed monoenergetic neutron beam. A standard configuration with an incident wavelength of 5.45 Å was used for the measurements. This configuration resulted in an energy resolution of 80−110 μeV (full width at half-maximum of the energy resolution, depending slightly on the scattering angle). By measuring the sample at a temperature of 1.5 K, the resolution of Pelican was estimated. For that procedure, it was assumed that all molecular motions and vibrations are frozen in addition to zero-point quantum fluctuations. Detectors in the angle range of 14°−119° were used for analysis leading to an (elastic) q range of 0.28−1.99 Å^{-1}.

For data reduction, the program LAMP[50] was used. The reduction includes an empty cell subtraction, conversion of the TOF to energy transfer, and vanadium normalization. A flat-plane self-shielding correction was appended by using a self-written Python script. In the primary data reduction, no rebinning of the TOF scale was done, and no regrouping to constant q. For the Fourier transform (see below) data were later interpolated to constant q, but the nonequidistant energy scale was preserved to avoid interpolation or binning-induced errors. Figure 3a depicts an example of a measurement at the Pelican. $S_{Inc}(q,\Delta E)$ shows broadening when measured at higher temperatures compared to the resolution. This effect is due to the onset of molecular fluctuations in the sample.

For the backscattering part of the quasielastic measurements, again the spectrometer IN16B was employed in the same high flux configuration as discussed for the elastic scans above. The employed configuration gives a resolution of ca. 0.8 μeV estimated by measurement of the sample at a temperature of 1.8 K under the same assumption discussed for Pelican. The energy range was given by the maximal speed of the Doppler drive by −29 to +29 μeV. The program Mantid was used for data reduction.[51] The background from an empty sample cell was eliminated by a Paalman−Pings angle-dependent empty cell subtraction with flat-plane shielding coefficients, and the spectra were normalized by a vanadium run. An example of raw spectra measured at IN16B is depicted in Figure 3b. Like for the time-of-flight experiments, the broadening of the spectra is due to molecular motions.

3. RESULTS AND DISCUSSION

Molecular fluctuations on the microscopic length and time scales are sensed by quasielastic neutron scattering experiments.[52] The wavelength and energy of the used cold neutrons define the accessible scales. The fundamental experimental quantity of quasielastic neutron experiments is the double differential cross-section

$$\frac{d^2\sigma}{d\Omega\, d\omega} = \frac{1}{4\pi}\frac{k_f}{k_i}(\sigma_{coh}S_{coh}(q,\omega) + \sigma_{inc}S_{Inc}(q,\omega)) \quad (1)$$

$\frac{d^2\sigma}{d\Omega\, d\omega}$ contains spatial and dynamic information on the underlying motional processes. Here ω denotes the angular frequency which is related to the measured energy transfer ΔE by $\Delta E = \hbar\omega$ ($\hbar$ is Planck's constant divided by 2π). Ω is the solid angle of detection. With regard to the neutron beam, $\mathbf{k}_i$ and $\mathbf{k}_f$ are the incident and final wave vectors of it, respectively. The scattering vector is defined by the vector difference of $\mathbf{q} = \mathbf{k}_f - \mathbf{k}_i$. In the following, only the modulus of the scattering vector, q, is used because the materials are macroscopically isotropic. σ_{coh} and σ_{inc} are the cross sections for coherent and incoherent scattering. They give the contrast in the experiment. $S_{coh}(q,\omega)$ and $S_{Inc}(q,\omega)$ are the coherent and incoherent dynamic scattering functions (dynamic structure factors) where their contributions to the double differential cross

https://doi.org/10.1021/acs.macromol.4c01045
Macromolecules 2024, 57, 8562−8575

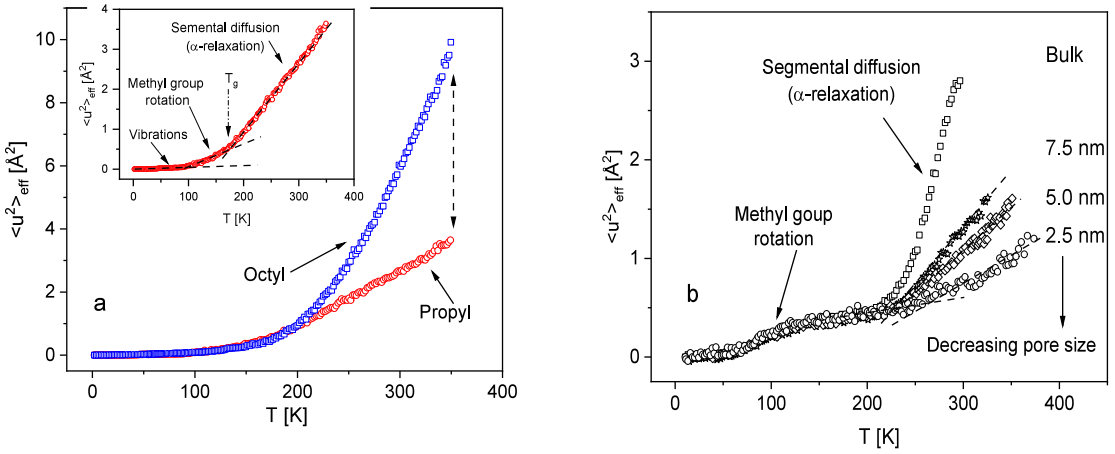

Figure 4. (a) Comparison of the temperature dependencies of the effective mean-squared displacement $\langle u^2\rangle_{eff}$ for PTCNSiOPr (red circles) and PTCNSiOOc (blue squares). The inset gives the temperature dependence of $\langle u^2\rangle_{eff}$ for PTCNSiOPr. Dashed lines are guides for the eyes. (b) Temperature dependence of the effective mean-squared displacement for poly(methylphenylsiloxane) nanoconfined to nanoporous sol−gel glasses at the indicated pore sizes. The data were taken from refs 55 and 56. It should be noted that the absolute values of the effective mean-squared displacement given in parts a and b cannot be compared directly as different methods for data analysis have been used for the two different systems.

section are weighted by σ_{coh} and σ_{inc}, respectively. $S_{Inc}(q,\omega)$ is caused by self-correlations of a particle while the coherent contribution $S_{coh}(q,\omega)$ is due to two-particle correlations. As shown by Figure 1 both considered polymers consist of carbon (C), hydrogen (H), and silicon (Si) as well as oxygen (O). The calculation of the scattering cross section for PTCNSiOPr and PTCNSiOOc is given in the Supporting Information of ref 41. For PTCNSiOPr, this calculation gives σ_{coh} = 171 barn and σ_{inc} = 2568.3 barn per monomeric unit. For PTCNSiOOc 306.7 barn and 4976.2 barn were estimated for σ_{coh} and σ_{inc}, respectively. The larger value of σ_{inc} compared to σ_{coh} indicates that the measured scattering is more than 90% incoherent. Moreover, in ref 41 it was calculated that the majority is due to the alkyl side chains as the most hydrogen nuclei are located there.

Elastic Scans. From the measured elastically scattered intensity $I_{el}(q)$ an effective mean-squared displacement $\langle u^2\rangle_{eff}$ is calculated by fitting the formula

$$\frac{I_{el}(q)}{I_0(q)} = \exp\left(-\frac{\langle u^2\rangle_{eff} q^2/3}{1 + \alpha_2\langle u^2\rangle_{eff} q^2/6}\right) \quad (2)$$

to $I_{el}(q)$ where I_0 is the total scattered intensity measured at the lowest accessed temperature. In eq 2 α_2 denotes an effective non-Gaussianity parameter, which is included to consider deviations of the data from the conventional Gaussian approach. The incorporation of multiple scattering effects into eq 2 is given in the Supporting Information (paragraph multiple scattering corrections of elastic scans). Compared to the standard Gaussian model this function is more reliable when $\langle u^2\rangle_{eff}$ becomes large. Moreover, no specific model is assumed like in ref 53. Up to the order of q^4 this expression is equivalent to the cumulant expansion with a non-Gaussianity parameter α_2. But it avoids the increase above 1 which occurs if the expansion is simply truncated after the q^4 term. Equation 2 is further motivated by the Singwi−Sjölander approach to the intermediate scattering function.[54]

The inset of Figure 4a gives the temperature dependence of the effective mean-squared displacement for PTCNSiOPr. At low temperature $\langle u^2\rangle_{eff}(T)$ is due to vibrations including the Boson peak.[41] At ca. 100 K the methyl group rotation sets in leading to a change in the temperature dependence of the effective mean-squared displacement. A further change of $\langle u^2\rangle_{eff}(T)$ is observed at ca. 165 K, which is due to the onset of the glass transition of the alkyl chain-rich domains. From the kink in the temperature dependence of $\langle u^2\rangle_{eff}$ a glass transition temperature of 167 K can be roughly extracted. This value corresponds to a glass transition temperature value estimated from the temperature dependence of the dynamic glass transition (α-relaxation) of the alkyl chain-rich domains at a frequency of 10^{-2} Hz (163 K).[24] The increase in $\langle u^2\rangle_{eff}$ at temperatures above the glass transition temperature is due to the diffusion of the hydrogen atoms of the alkyl chains in their domains.

Figure 4a compares the temperature dependence of the mean-squared displacements for PTCNSiOPr and PTCNSiOOc. For both materials, the onset of the methyl group rotation is observed around 100 K. At higher temperatures, the glass transition of the alkyl side chain-rich domains is observed like for PTCNSiOPr also for PTCNSiOOc. The estimated value of the glass transition temperature from the elastic scans is higher for PTCNSiOOc in comparison to PTCNSiOPr and agrees with the data obtained by dielectric and thermal spectroscopy as well as by DSC.

The main difference in the temperature dependence of the elastic scans is that for PTCNSiOOc the effective mean-squared displacement increases much stronger than for PTCNSiOPr, resulting in much higher values for $\langle u^2\rangle_{eff,PTCNSiOOc}$. This behavior cannot be explained by the higher number of protons in the alkyl side chain-rich domains of PTCNSiOOc compared to that of PTCNSiOPr (see Figure S1 in the Supporting Information). The dependence of $\langle u^2\rangle_{eff}$ of PTCNSiOR with decreasing alkyl chain length, or in other words with decreasing size of the alkyl chain-rich domains, resembles in some way the temperature dependence of the mean-squared displacement of poly(methylphenylsiloxane) confined to nanoporous glasses (see Figure 4b).[52,53] For that system, the value of the effective mean-squared displacement at temperatures above the glass transition temperature decreases systematically with decreasing pore size. Therefore, it can be concluded that the segmental diffusion in the alkyl chain-rich

https://doi.org/10.1021/acs.macromol.4c01045
Macromolecules 2024, 57, 8562−8575

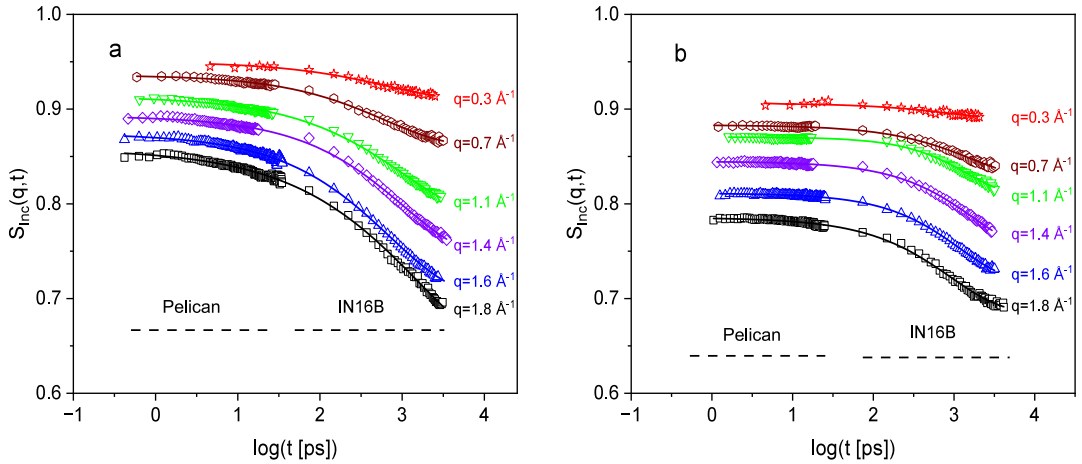

Figure 5. Incoherent intermediate scattering function $S_{Inc}(q,t)$ for PTCNSiOPr (a) and PTCNSiOOc (b) versus time for the indicated q vector at T = 150 K. The solid lines are fit of eq 3 to the data. The time ranges measured by both spectrometers are indicated. The shift of $S_{Inc}(q,t)$ to lower values with increasing q vector is due to the q dependence of the Debye−Waller factor. The errors in the data are smaller than the size of the symbols.

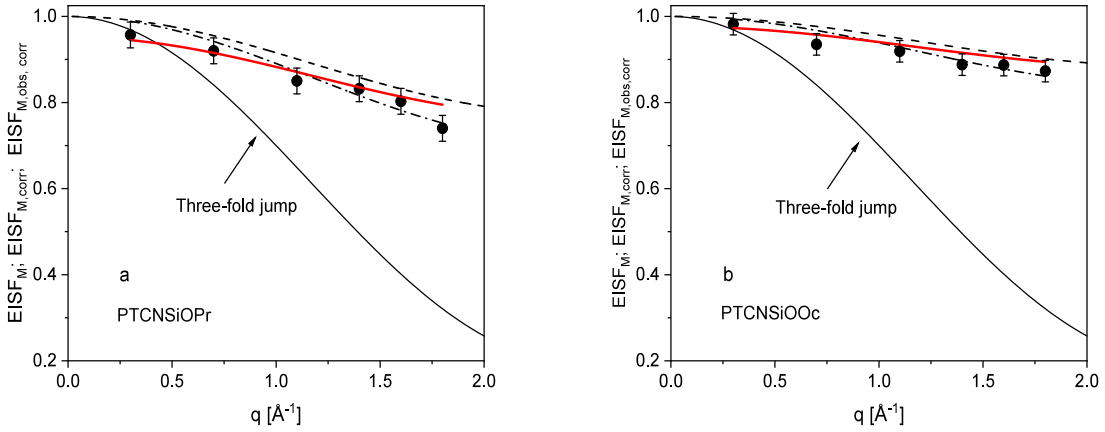

Figure 6. $EISF_M$, $EISF_{M,corr}$, and $EISF_{M,obs,corr}$ versus scattering vector q for PTCNSiOPr (a) and PTCNSiOOc (b). The solid black line is calculated from eq 4. The dashed line is the dependence calculated with theoretical value of C_{fix} due to the chemical structure of the repeating unit according to eq 5b. The dashed dotted line is the fit of eq 5b leading to C_{fix} fitted (see Table 2). The red line is the calculated dependence according to eq 6b with the values of the parameters given in Table 2. Typical errors of the data resulting from the fit of eq 3 are included in the figure.

domains of the PTCNSiOR is confined as the glass transition temperature of the polynorbornene backbone-rich matrix is high (see ref 24). This conclusion will be discussed further in this work. From the effective mean-squared displacement measured at the highest temperature a maximal diffusion distance can be calculated by $\sqrt{\langle u^2\rangle_{eff}}$ for the time scale given by the resolution of the backscattering spectrometer (ca. 2 ns). A maximal diffusion distance of 0.31 nm is obtained for PTCNSiOOc and 0.19 nm for PTCNSiOPr. These values are much smaller than the size of the alkyl side chain-rich domains (see Table 1). This is the reason no saturation in the temperature dependence of $\langle u^2\rangle_{eff}$ is observed due to the finite domain size. The molecular origin for these small diffusion distances might be that alkyl chains are grafted to the backbone. This fact will limit the diffusion of the alkyl side chains. The effect of the grafting of the alkyl chains to the backbone is further addressed in the QENS section. Nevertheless, the lower value obtained for PTCNSiOPr in comparison to that calculated for PTCNSiOOc might point again to confinement effects. This point is further discussed in the QENS section. It is worth noting that a similar behavior $\langle u^2\rangle_{eff}$ with regard to the pore size was observed for poly(methylphenylsiloxane) confined to nanoporous glasses were the diffusion of the segments is not restricted by a grafting of the chains to the pore walls.[52,53]

Quasielastic Scattering. *Methyl Group Rotation.* As the difference in the energy resolution of time-of-flight and backscattering is large (see Figure 3) both measurements cannot be jointly discussed in the energy domain as measured. Therefore, the dynamic scattering functions $S(q,\omega)$ obtained from time-of-flight and backscattering were Fourier transformed $S(q,t) = (1/2\pi)\int_{-\infty}^{\infty} S(q,\omega)\exp(-i\omega t)\,d\omega$ (i is the imaginary unit) and divided by the corresponding Fourier transform of the resolution to discuss the results together in the time domain. By this procedure, the incoherent intermediate scattering function $S_{Inc}(q,t)$ was obtained in absolute values. For this calculation the self-written program "unift" was used.[57]

Figures 5a and 5b depict $S_{Inc}(q,t)$ for PTCNSiOPr and PTCNSiOOc for 150 K for different q vectors, respectively. First, Figure 5 shows that the data from Pelican and IN16B

https://doi.org/10.1021/acs.macromol.4c01045
Macromolecules 2024, 57, 8562−8575

Table 2. Parameters for the Methyl Group Rotation[a]

code	hydrogens in the repeating unit	hydrogens in the methyl groups	C_{fix} theoretical	C_{fix} fitted	s	C_{fix} MS corrected	E_A [kJ/mol]
PTCNSiOPr	32	9	0.718	0.64	0.18	0.72	8.6
PTCNSiOOc	62	9	0.855	0.80	0.16	0.85	7.9

[a]The definition of C_{fix} is given by eq 5a. The definition of s is given in eq 6a. The error in C_{fix} fitted and C_{fix} MS corrected is 0.005, the errors of s are 0.005, and the activation energy of the methyl group rotation is 1 kJ/mol.

agree regarding their functional shape in the time domain and can be now jointly analyzed.

A single decay in $S_{Inc}(q,t)$ with time is observed for both materials which corresponds to the methyl group rotation (see Figure 4a). In principle, the methyl group rotation is well understood by the rotation rate distribution model (RRDM).[58] Here in a simplified approach a stretched exponential function is utilized to analyze $S_{Inc}(q,t)$ for the methyl group rotation which reads

$$S_{Inc}(q,t) = DWF \cdot S_{Inc,methyl}(q,t) = DWF\left((1 - EISF_M(q)) \times \exp\left(-\left(\frac{t}{\tau_M}\right)^{\beta_M}\right) + EISF_M(q)\right) \quad (3)$$

τ_M denotes the relaxation time for the methyl group rotation, and β_M is the stretching parameter. $EISF_M(q)$ is the elastic incoherent structure factor for the methyl group rotation, and DWF symbolizes the Debye–Waller factor DWF = $\exp(-q^2\langle u_{fast}^2\rangle/3)$ where $\langle u_{fast}^2\rangle$ is a mean-squared displacement due to fast processes like vibrations. The fit lines in Figure 5 evidence that the data can be well described by eq 3.

Most straightforwardly, the dependence of the elastic incoherent structure factor for the methyl group rotation can be described by a jump-diffusion in a 3-fold potential $V(\phi) \sim (1 - \cos(3\phi))/2$.[55,59] This potential has three equivalent energy minima regarding the rotational angle ϕ of the methyl group. The $EISF_M$ of the methyl group rotation is then calculated to

$$EISF_M(q) = \frac{1}{3}\left(1 + 2\frac{\sin(\sqrt{3}qr)}{\sqrt{3}qr}\right) \quad (4)$$

where r is the radius of the circle spanned by the positions of the hydrogens in the methyl group which has the value of 1.027 Å. The elastic incoherent structure factor for the methyl group rotation as obtained from the fits of eq 3 is plotted versus the scattering vector q in Figure 6 for PTCNSiOPr (a) and PTCNSiOOc (b). When the q dependence of the experimental data is compared with that calculated by eq 4, it is observed that the experimental results do not obey the theoretical prediction. To understand the different q dependencies, one has to consider the number of hydrogens in the methyl groups that undergo the methyl rotation, in comparison to all hydrogen nuclei in the repeating unit. PTCNSiOPr has 32 hydrogen nuclei in the repeating unit while only 9 of them are in the three methyl groups (see Table 2). For that reason, 23 hydrogen nuclei are not involved in the methyl group rotation. They will scatter elastically in the temperature range where the methyl group rotation becomes active. For PTCNSiOOc the situation is 62 hydrogens in the repeating unit compared to 9 protons in the methyl groups.

The number fraction of hydrogen nuclei that scatter elastically C_{fix} is calculated from the chemical structure of the repeating unit of both polymers by

$$C_{fix} = (H_{repeating\ unit} - H_{methyl\ groups})/H_{repeating\ unit} \quad (5a)$$

The number fraction of elastically scattering hydrogens rescales the result of eq 4 by[37,38,52,60]

$$EISF_{M,corr}(q) = (1 - C_{fix})EISF_M(q) + C_{fix} \quad (5b)$$

First, it was concluded that the experimental data points cannot be exactly described by eq 5b with the value of C_{fix} due to the chemical structure of the repeating unit. Therefore, eq 5b is fitted to the experimental values of the elastic incoherent structure factor. Figure 6 shows that the experimental data points can be approximately described by fitting eq 5b to the data but this procedure leads to values of C_{fix} which are in the frame of the error bars essentially smaller than the theoretical ones calculated from the chemical structure of the repeating unit (see Table 2). Moreover, there is a systematic deviation of the experimental data from the prediction that $S_{Inc}(q)$ should approach 1 for $q \to 0$. These deviations are most probably due to multiple scattering which are approximately in the order of 10% for both materials.[61] Therefore, an apparent elastic incoherent structure factor $EISF_{M,obs}$ is estimated including multiple scattering contributions.[52] The whole procedure is given in the appendix of ref 52 and is similar to the procedure given elsewhere.[50,62] This approach is based on summing the multiple scattering contributions of all orders. It results in

$$EISF_{M,obs}(q) = (1 - s)\left(EISF_M(q) + \frac{s\bar{A}^2}{1 - s\bar{A}}\right) \quad (6a)$$

s denotes the probability that a neutron is scattered again, and $\bar{A}$ is the average of the $EISF_M$ over the solid angle. The integration of eq 4 gives $\bar{A} = 0.543$. Here a misspelling in the numerical value of $\bar{A}$ given in ref 52 is corrected.

The multiple scattering correction has to be also applied to eq 5b. As elaborated in the Supporting Information of ref 52 one obtains

$$EISF_{M,obs,corr}(q) = (1 - s)\left((1 - C_{fix})EISF_M(q) + C_{fix} + \frac{s(\bar{A} + (1 - \bar{A})C_{fix})^2}{1 - (\bar{A} + (1 - \bar{A})C_{fix})s}\right) \quad (6b)$$

A fit of eq 6b to the estimated EISF values with C_{fix} and s as free parameters leads to reasonable values of the multi-scattering parameter s and of fractions of fixed, elastically scattering hydrogens which correspond to that calculated from the chemical structure of repeating unit (see Figure 6 and Table 2).

In conclusion of the paragraph, the methyl group rotation in the Janus polynorbornenes was analyzed in terms of a jump diffusion in a 3-fold potential with three equivalent energy

https://doi.org/10.1021/acs.macromol.4c01045
Macromolecules 2024, 57, 8562−8575

minima. This approach leads to a correct description of the q dependence of elastic incoherent structure factor when the number of the hydrogens is considered which takes part in the methyl group rotation and multiple scattering corrections are carried out.

Segmental Diffusion (Structural Relaxation of the Alkyl Chain-Rich Domains). Figure 7 gives the elastically scattered intensity I_{el} at q = 1.84 Å^{-1} normalized by the total elastically scattered intensity I_0 measured during the elastic fixed windows scans versus temperature. The temperature dependence of the elastically scattered intensity shows a major difference between those of PTCNSiOPr and PTCNSiOOc. While for PTCNSiOOc the elastically scattered intensity decays to zero for the highest temperature measured by the quasielastic measurements, PTCNSiOPr partly scatters still elastically ($I_{el}/I_0 > 0$). As discussed in the Introduction this behavior can be rationalized by assuming that for PTCNSiOPr the alkyl chain-rich domains are surrounded by a matrix consisting of the polynorbornene backbone structures. As the glass transition temperature of the backbone-rich matrix is found by fast scanning calorimetry to be ca. 675 K at a heating rate of 5000 K/s, the hydrogens in the matrix are immobile at the temperatures covered by the quasielastic neutron experiments and scatter elastically.[24] For PTCNSiOOc the alkyl chain-rich domains percolate through the system and backbone-rich domains floating in the percolated alkyl chain phase. Therefore, the elastically scattered intensity decays to nearly zero.

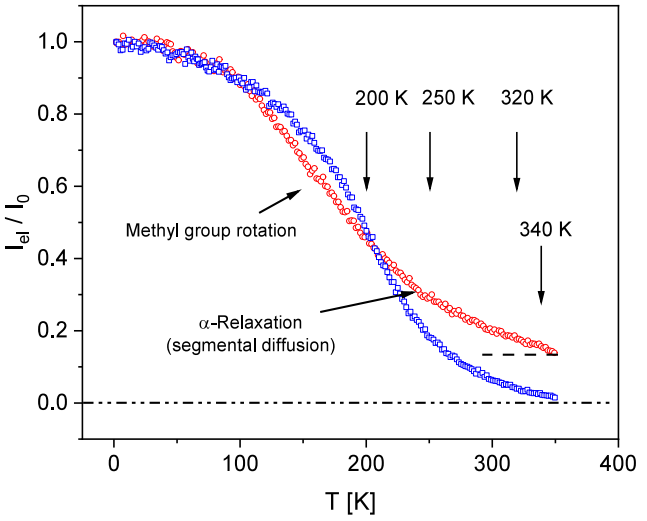

Figure 7. Elastically scattered intensity I_{el} at q = 1.84 Å^{-1} normalized by the elastically scattered intensity at $T \approx 2$ K, I_0, versus temperature for PTCNSiOPr (red circles) and PTCNSiOOc (blue squares). The arrows indicate the temperatures for which QENS was carried out to analyze the segmental dynamics (at 340 K measurements were conducted only for PTCNSiOPr).

Figure 8 depicts the incoherent intermediate scattering function for the considered PTCNSiORs versus time at T = 250 K. Like for the methyl group rotation, the data obtained from Pelican and IN16B can be well compared in the time domain. The different scattering behavior for both materials can be also observed in the time dependence of the incoherent intermediate scattering function. For PTCNSiOOc (Figure 8b) $S_{Inc}(q,t)$ decays strongly with time. For PTCNSiOPr (Figure 8a) the incoherent intermediate scattering function decays weaker than for PTCNSiOOc showing a kind of plateau for the longest times. This plateau might be due to the elastic scattering of the polynorbornene backbone-rich matrix, while the decay is due to the relaxation processes in the alkyl chain-rich domains.

For temperatures above 150 K, the time dependence of $S_{Inc}(q,t)$ is due to both the methyl group rotation and the segmental dynamics (α-relaxation, segmental diffusion) in the alkyl chain-rich domains. If two relaxation processes are present in the measured spectra, their scattering functions are convoluted in the energy or frequency domain. After the Fourier transformation, the convolution leads to a product in the time domain. For that reason, the whole scattering law is written as

$$S_{Inc}(q,t) = \mathrm{DWF}\cdot S_{Inc,whole}(q,t) = \mathrm{DWF}\cdot S_{Inc,methyl}(q,t)\cdot S_{Inc,segmental}(q,t) \quad (7)$$

For processes with well-separated relaxation times, the product might be simplified by a sum.[52,63] As Figure 8 shows, this is not the case here. Therefore, the exact product is further used to analyze the data.

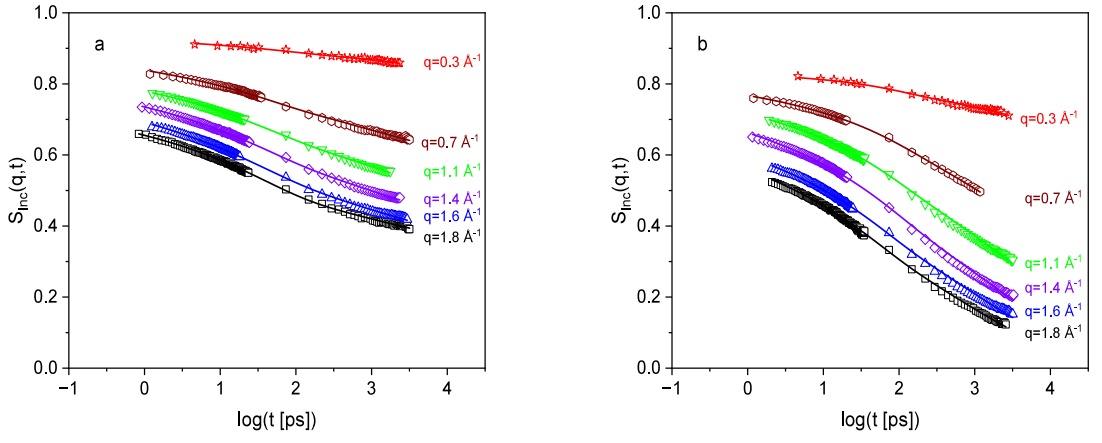

Figure 8. Incoherent intermediate scattering function $S_{Inc}(q,t)$ for PTCNSiOPr (a) and PTCNSiOOc (b) versus time for the indicated q vectors at T = 250 K. The shift of $S_{Inc}(q,t)$ to lower values with increasing q vector is due to the q dependence of the Debye−Waller factor. The errors of the data are smaller than the size of the symbols. The solid lines are fits of eq 9 to the data. For details, see text.

https://doi.org/10.1021/acs.macromol.4c01045
Macromolecules 2024, 57, 8562−8575

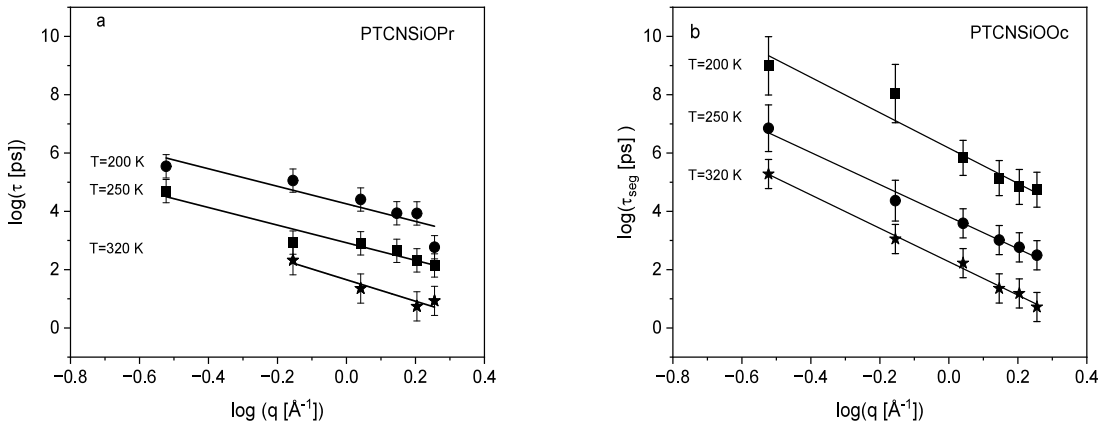

Figure 9. Segmental relaxation time τ_{seg} versus q vector at the indicated temperatures for PTCNSiOPr (a) and (b) and PTCNSiOOc. Lines are linear regressions to the data. For PTCNSiOPr the data for the lowest q vector could not be unambiguously analyzed.

According to ref 64, for traditional diffusion processes which can be described by a diffusion coefficient D, the effective mean-squared displacement increases linearly with time, $\langle u^2\rangle_{eff} = 3Dt$. Then for the intermediate incoherent scattering function follows[52,61]

$$S_{Inc,segmental}(q, t) = \exp(-q^2Dt) = \exp\left(-\frac{t}{\tau_{seg}}\right) \quad (8a)$$

Here τ_{seg} is the relaxation time $\tau_{seg} = D^{-1}q^{-2}$. Equation 8a assumes that the details of the molecular motions are averaged out. Therefore, it is valid for a long time and large spatial scales (small q values). It is known for instance from broadband dielectric spectroscopy that the relaxation function for the α-relaxation does not follow an exponential decay (see for instance refs 65−67 and references cited therein). This is also true for the intermediate incoherent scattering function measured by quasielastic neutron scattering.[64,68,69] Such behavior can be modeled by a sublinear diffusion $\langle u^2\rangle_{eff} \sim t^{\beta_{seg}}$. This assumption leads to the intermediate scattering function

$$S_{Inc,segmental}(q, t) = \exp\left(-\left(\frac{t}{\tilde{D}^{-1/\beta_{seg}}q^{-2/\beta_{seg}}}\right)^{\beta_{seg}}\right) = \exp\left(-\left(\frac{t}{\tau_{seg}}\right)^{\beta_{seg}}\right) \quad (8b)$$

$\tilde{D}$ is related to the diffusion coefficient, and β_{seg} is the shape parameter for the α-relaxation. The segmental relaxation time $\tau_{seg}(T,q)$ is then given by $\tau_{seg} = \tilde{D}^{-1/\beta_{seg}}q^{-2/\beta_{seg}} = \tau_1(T)q^{-Slope}$ with $Slope = 2/\beta_{seg}$. The temperature dependence of the relaxation time is given by $\tau_1(T)$ taken at a value of the q vector of ca. 1 Å^{-1}. It was found in the literature that for a q vector value of ca. 1 Å^{-1} the neutron data agree approximately with that obtained by dielectric spectroscopy.[52]

At least for PTCNSiOPr an elastic scattering contribution must be considered. This contribution might be modeled by a second elastic incoherent structure factor $EISF_{matrix}$ for the polynorbornene backbone-rich matrix. Then eq 7 is rewritten as

$$S_{Inc}(q, t) = DWF((1 - EISF_{matrix})S_{Inc,whole}(q, t) + EISF_{matrix}) \quad (9)$$

For PTCNSiOOc no $EISF_{matrix}$ must be taken into consideration as the alkyl side chain-rich domains percolate through the matrix.

The intermediate incoherent scattering function shown in Figure 8 displays a structure-less decay. Therefore, for the fitting of eq 9 to the data, some minimal set of assumptions must be made to minimize the number of free fit parameters. The elastic incoherent structure factor for the methyl group rotation is taken from the measurements at 150 K for all temperature above 150 K. This also concerns the shape parameter for the methyl group rotation β_M were an arithmetical average over all values of q was taken (β_M = 0.77). The shape parameter for the α-relaxation β_{seg} is taken from the analysis of the dielectric spectra by the model function of Havriliak−Negami in ref 24 where $\gamma_{HN} = 1$ (symmetrical relaxation function) is assumed. To calculate β_{seg} from the estimated β_{HN}, the approximation of Colmenero et al. $\beta_{seg} = (\beta_{HN}\gamma_{HN})^{0.81}$ is used.[70] The used values are given in the Supporting Information. For PTCNSiOOc, $EISF_{Matrix}$ is set to zero as the alkyl side-chain-rich domains percolates through the backbone-rich matrix. The used parameters are given in the Supporting Information (Tables S1 and S2). Figure 8 shows that the data can be nicely described by that approach. From the fits, the relaxation time τ_{seg} for the α-relaxation is obtained.

In the following, first the dependence of the segmental relaxation times on the value of the q vector is discussed. Figure 9 gives the q dependence of the segmental relaxation time in a log−log plot. This plot shows that the data can be described by a straight line. The direct comparison of Figure 9a,b reveals a large difference in q dependence of the relaxation time of the segmental dynamics for both materials. From a linear regression to the data, the parameter *Slope* is obtained.

The obtained values of the *Slope* parameter are depicted versus temperature for both materials in Figure 10. If the q dependence of the segmental relaxation time fulfills the condition $Slope = 2/\beta_{seg}$ the underlying dynamics can be regarded as homogeneous while $Slope < 2/\beta_{seg}$ suggests heterogeneous molecular fluctuations. This line of argumentation was discussed for instance by Tyagi et al.[71] for poly(vinyl acetate) combining dielectric results with that obtained from quasielastic neutron scattering. Some further discussion concerning this topic can be also found in ref 72. The two limiting cases, $Slope = 2/\beta_{seg}$ for PTCNSiOPr and PTCNSiOOc as well as $Slope = 2$, are added to Figure 10.

For PTCNSiOPr the estimated values for the parameter *Slope* are much smaller than expected for a homogeneous diffusion (see the dashed red line in Figure 10). Therefore, it is concluded that the underlying molecular fluctuations are

https://doi.org/10.1021/acs.macromol.4c01045
Macromolecules 2024, 57, 8562−8575

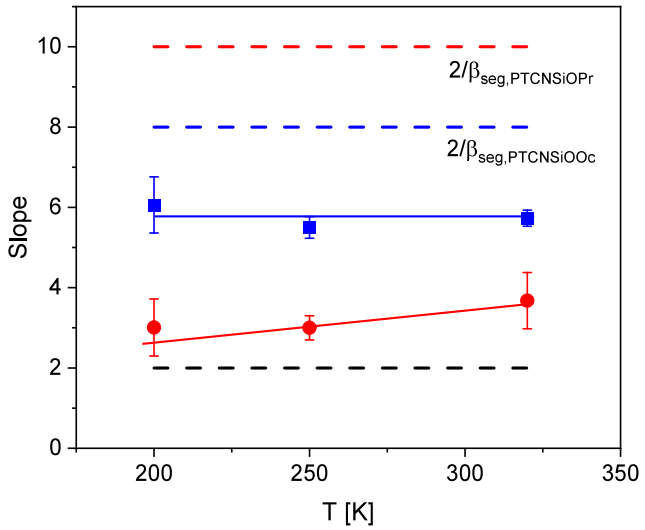

Figure 10. Parameter *Slope* vs temperature for PTCNSiOPr (red circles) and PTCNSiOOc (blue squares). The red and blue solid lines are guides to the eyes. The dashed red and blue lines are the limiting cases *Slope* = $2/\beta_{seg}$ are the limiting cases for homogeneous diffusion (red dashed line for PTCNSiOPr, blue dashed line PTCNSiOOc). The black dashed line is the limiting case for conventional diffusion ($\langle u^2\rangle_{eff} = 3Dt$; $\tau_{seg} = D^{-1}q^{-2}$; see discussion above). *Slope* = 2.

heterogeneous. Moreover, *Slope* seems to increase slightly with increasing temperature. This might mean that the molecular motions become more homogeneous with increasing temperature. (Alternatively, the data can be modeled with a constant value of ca. 3.2 but with a larger deviation.) The molecular reason for the heterogeneous diffusion can be discussed in two directions. First, the small size of the alkyl side chain-rich domains (see Table 1) may induce heterogeneous fluctuations. Second, for the considered Janus polynorbornenes the alkyl side chains are grafted onto the semirigid backbone. Therefore, the hydrogen nuclei in the alkyl side chain might be restricted in their molecular mobility in dependence on their distance from the main chain. This effect will also lead to a heterogeneous diffusion. In the case of PTCNSiOOc the diffusion is less heterogeneous compared to PTCNSiOPr. This effect is most probably related to the longer alkyl chains of PTCNSiOOc leading to larger alkyl chain-rich domains (see Table 1).

To compare the relaxation times obtained from the quasielastic neutron experiments with the dielectric relaxation or thermal data a mean relaxation time is calculated by

$$\tau(q, t) = \tau_{seg}(q, T)\cdot\Gamma(1/\beta_{seg})/\beta_{seg} \quad (10)$$

Here $\Gamma(x)$ symbolizes the Gamma (Euler) function. In Figure 11 the relaxation rates f_p obtained from the neutron scattering experiments are plotted together with the dielectric and thermal data ($f_p = 1/(2\pi\tau)$). Both latter data sets are taken from ref 24. It is known that the temperature dependence of relaxation rates of the segmental dynamics can be described by the Vogel−Fulcher−Tammann (VFT) equation which reads[73−75]

$$\log f_p(T) = \log f_\infty - \frac{DT_0}{T - T_0} \quad (11)$$

Here f_∞ is the relaxation rate at infinitely high temperatures. T_0 symbolizes the ideal glass transition of the Vogel temperature which is found to be 50−70 K below the glass transition temperature measured by conventional DSC. D is the so-called fragility parameter or fragility strength which can be used to classify and compare glass forming systems.[76] As discussed in ref 24, the temperature dependence of dielectric and thermal relaxation rates can be well approximated by a VFT equation. The relaxation rates obtained by neutron spectroscopy match in both their absolute values and their temperature dependencies the data obtained by dielectric and thermal measurements (see Figure 11). The temperature dependence of the relaxation rates obtained by the different methods can be well described by a common VFT dependence, including the relaxation rate for the neutron data at a q value of 1 Å^{-1} into the fit. This agreement proves that the same molecular process is sensed by dielectric/thermal measurements as well as by neutron spectroscopy. Moreover, it might be concluded from

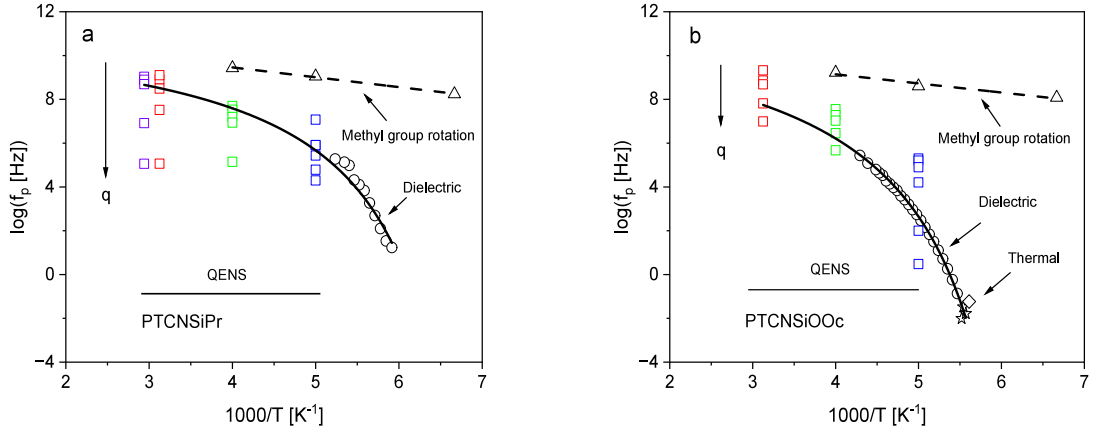

Figure 11. Relaxation rates f_p vs inverse temperature for PTCNCSiOPr (a) and PTCNSiOOc (b). The colored squares are the neutron data for the different q values. The different colors represent the different measurement temperatures. Open circles are the dielectric data, open stars are data obtained by temperature-modulated DSC measurements, and diamonds are calculated from conventional DSC measurements. The solid line is a fit of the VFT equation including interpolated the neutron data at a q vector value of 1 Å^{-1} as it was found in the literature that for a q vector value of ca. 1 Å^{-1} the neutron data agree approximately with that obtained by dielectric spectroscopy.[52] For the errors in the neutron relaxation time of the segmental relaxation, see Figure 9. The triangles are data obtained for the methyl group rotation. The dashed line is a fit of the Arrhenius equation to the data of the methyl group rotation.

https://doi.org/10.1021/acs.macromol.4c01045
Macromolecules 2024, 57, 8562−8575

Figure 11 in the frame of the fragility approach that the segmental dynamics shows stronger behavior for PTCNSiOOc in comparison to that of PTCNSiOPr.

An analysis of the obtained values for $EISF_{Matrix}$ shows that the elastic contribution is larger than that one would expected simply from the fraction of hydrogens in the polymer backbone $BG = (H_{monomeric\ unit} - H_{akyl\ side\text{-}chain})/H_{monomeric\ unit} = 0.342$ (see Figure S2) which are immobilized at the considered temperatures and time scales. It is assumed that the higher elastic contribution is due to a boundary layer, which is related to the grafting of the alkyl chains to the backbone. In Figure 12 the

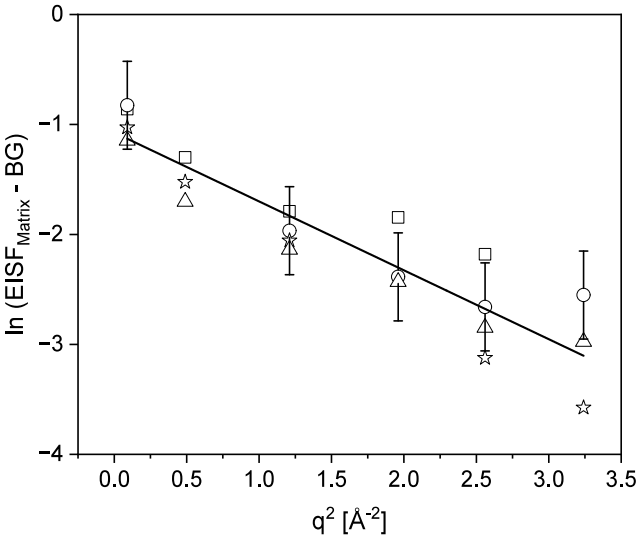

Figure 12. $\ln(_{EISFMatrix} - BG)$ versus the scattering vector q^2 for PTCNSiPr: squares, 200 K; circles, 250 K; asterisks, 320 K; and triangles, 340 K. BG = 0.342. For estimation of BG see text. Typical errors are included in the figure. The solid line is a linear regression to all of the data points.

elastic excess contribution, $\ln(EISF_{matrix} - BG)$, is depicted versus q^2 for PTCNSiOPr. Although the data have a larger scatter, it can be described by a straight line. This means that the q dependence of the $EISF_{matrix}$ follows the dependence $\exp(-a^2q^2)$, where a is a characteristic length scale which can be considered as the discussed boundary layer to which the dynamics of the alkyl side chains is confined by the grafting to the backbone-rich domains. From the fit a value $a = 1.26 \pm 0.3$ Å is estimated. This value corresponds roughly to one or two carbon lengths in sp^3 hybridization. This value has a reasonable order of magnitude for such a boundary layer as this layer is due to the grafting of the alkyl side chain to immobilized polynorbornene backbone. For PTCNSiOOc the alkyl side-chain-rich domains percolate through the backbone-rich matrix. Therefore, such a boundary layer does not exist. As discussed in ref 24 the polynorbornene backbone is somewhat plasticized by the alkyl side chains and have therefore some molecular mobility.

In concluding this section, the segmental diffusion of the alkyl side chains in the alkyl side-chain-rich domains was analyzed by assuming a sublinear diffusion. As segmental diffusion closely overlaps with the methyl group rotation, the latter must be included in the analysis. To this aim, the product of the scattering functions of the methyl rotation and of the segmental diffusion was considered as the scattering law. From the dependence of the relaxation time on the q vector, the heterogeneity of the segmental diffusion was inferred. It was found that the segmental diffusion is more heterogeneous for PTCNSiOPr in comparison to PTCNSiOOc.

The temperature dependence of the relaxation rates obtained from the segmental diffusion by quasi-elastic neutron scattering agrees with those measured by dielectric spectroscopy and dynamic calorimetry.

From the analysis of $S_{inc}(q,t)$ also, the relaxation time for the methyl group rotation can be deduced. The methyl group rotation is a localized process. Therefore, in difference to the α-relaxation, the relaxation time of the methyl group rotation is not dependent on the q vector. For that reason, a value which is arithmetically averaged over all q vectors is considered. The obtained data are listed in Figure 11. The temperature dependence of the relaxation rates is linear when plotted versus inverse temperature and can be described by the Arrhenius equation

$$f_p(T) = f_\infty \exp\left(-\frac{E_A}{RT}\right) \tag{12}$$

E_A denotes the activation energy, and R is the general gas constant. The estimated activation energies are listed in Table 2. The difference in the activation energy for the methyl group rotation for both compound is within the error of the measurements, which is 1 kJ/mol. Therefore, the values can be considered as similar as it should be expected for the localized methyl group rotation. Nevertheless, the slightly higher value of the activation energy obtained for PTCNSiOPr in comparison to PTCNSiOOc might be due to the smaller size of the alkyl side chain-rich domains which may hinder the methyl group rotation due to a stronger restriction exerted by the surrounding more rigid backbone-rich phase.

4. CONCLUSION

Quasielastic neutron scattering was employed to investigate the molecular dynamics of homologous Janus polynorbornenes with flexible $-Si(OR)_3$ side chains on microscopic time and length scales. Here two different lengths of side chains (propyl and octyl) of these poly(tricyclononenes) are considered. The polymers were denoted as PTCNSiOPr and PTCNSiOOc. These polymers have some potential in the field of green gas separation, especially for the separation of higher hydrocarbons.

In a previous work by some of the authors, it was shown by employing X-ray scattering that these polymers undergo a nanophase separation into alkyl side-chain-rich and backbone-rich domains. The size of the alkyl side chain-rich domains increases with the length of the alkyl side chain. Furthermore, it was shown by broadband dielectric and thermal spectroscopy that the alkyl side chain-rich domains undergo a glass transition.

To have a reasonably broad time range for the quasielastic neutron scattering experiments (QENS), neutron time-of-flight (TOF) and neutron backscattering were combined. The spectra obtained by both methods were Fourier transformed and divided by the Fourier transform of the corresponding resolution. In that way, absolute values of the intermediate scattering function $S_{Inc.}(q,t)$ were obtained in the time domain. Therefore, the data obtained from the TOF and the backscattering could be jointly analyzed. For the TOF experiments, Pelican (ANSTO, Sydney, Australia) was used.

https://doi.org/10.1021/acs.macromol.4c01045
Macromolecules 2024, 57, 8562−8575

For the backscattering part of the experiment, IN16B (Institut Laue-Langevin, Grenoble, France) was employed.

To have an overview of the molecular dynamics, fixed elastic window scans were measured employing the backscattering spectrometer IN16B with the Doppler at rest ($\Delta E \approx 0$). By these measurements, the molecular motions were sensed on a time scale that corresponds to the resolution of IN16B (ca. 2 ns). The temperature dependence of the estimated effective mean-squared displacement $\langle u^2 \rangle_{\text{eff}}$ shows different processes, vibrations at the lowest temperatures, and the methyl group rotation that sets in at temperatures around 100 K. At temperatures above the glass transition temperature of the alkyl side chain-rich domains, the segmental diffusion can be observed in the effective mean-squared displacement. Comparing the temperature dependence of PTCNSiOPr and PTCNSiOOc at temperatures above the respective glass transition temperatures reveals that $\langle u^2 \rangle_{\text{eff}}$ of the former Janus polymer is much smaller than that for PTCNSiOOc which cannot be explained by the different number of protons involved in the process. Moreover, the maximal diffusion distance is calculated from the mean-squared displacement measured at the highest temperature. The estimated value for PTCNSiOPr is smaller than that for PTCNSiOOc. The molecular reason is probably that the alkyl chains are grafted to the rigid backbone, which limits the diffusion of the alkyl side. Nevertheless, the dependence of the effective mean-squared displacement on the length of the alkyl side chain resembles in some way the behavior of a polymer confined to nanoporous glasses with a decreasing pore diameter. Therefore, it might be concluded that for PTCNSiOR the segmental diffusion of the alkyl side chain in its domains is confined to some extent. The confinement effect is larger for PTCNSiOPr in comparison to PTCNSiOOc.

For the QENS experiment at the lowest temperature (150 K), the time dependence of $S_{\text{Inc}}(q,t)$ is due to the methyl group rotation. $S_{\text{Inc}}(q,t)$ is analyzed by fitting a stretched exponential to the data. This fitting process results in a relaxation time and an elastic incoherent structure factor EISF_{M} for methyl group rotation. The q dependence of the EISF_{M} is discussed in a framework of jump-diffusion in a 3-fold potential. During this analysis it must be considered that not all hydrogens present in the repeating unit undergo the methyl group rotation as well as multiple scattering events must be considered. This analysis leads to a fraction of protons that are involved in the methyl group rotation consistent with the chemical structure of the repeat unit. For the activation energy of the methyl group rotation, reasonable values in the range of 8−9 kJ/mol were obtained.

For temperatures higher than 150 K the time dependence of $S_{\text{Inc}}(q,t)$ is due to methyl group rotation and segmental mobility. The segmental diffusion is modeled by a sublinear diffusion. Therefore, the product of two scattering functions, one for the methyl group rotation and one for the segmental diffusion, is fitted to the time dependence of $S_{\text{Inc}}(q,t)$. This process leads to the relaxation time for the segmental dynamics. The relaxation times of the segmental dynamics obtained by neutron scattering agree in their absolute values and their temperature dependence with that deduced by dielectric and thermal spectroscopy. In difference to the localized methyl group rotation, the relaxation time of the segmental dynamics depends on q as the segmental dynamics is a cooperative process. The q dependence of the relaxation of the segmental dynamics can be discussed by two limiting cases: homogeneous and heterogeneous diffusion. The analysis reveals that for the considered Janus polynorbornenes the segmental dynamics is heterogeneous. The heterogeneity is larger for PTCNSiOPr in comparison to PTCNSiOOc. The heterogeneity might be caused by the small size of the alkyl side chain-rich domains and/or by the fact the alkyl side-chains are grafted to a semirigid backbone.

The present work will be continued by analyzing inelastic fixed window scans (one offset energy) for the whole homologous series of the Janus poly(tricyclononenes).

■ ASSOCIATED CONTENT

Supporting Information

The Supporting Information is available free of charge at https://pubs.acs.org/doi/10.1021/acs.macromol.4c01045.

Scaling of the mean-squared displacement for the different numbers of hydrogens in the side chain; $\text{EISF}_{\text{matrix}}$ versus scattering vector; fixed parameters for the fits (PDF)

■ AUTHOR INFORMATION

Corresponding Author

Andreas Schönhals − *Bundesanstalt für Materialforschung und -prüfung (BAM), 12205 Berlin, Germany; Institut für Chemie, Technische Universität Berlin, 10623 Berlin, Germany;* orcid.org/0000-0003-4330-9107; Phone: +49 30/8104-3384; Email: Andreas.Schoenhals@bam.de; Fax: +49 30/8104-73384

Authors

Paulina Szymoniak − *Bundesanstalt für Materialforschung und -prüfung (BAM), 12205 Berlin, Germany*

Mohamed A. Kolmangadi − *Bundesanstalt für Materialforschung und -prüfung (BAM), 12205 Berlin, Germany;* orcid.org/0000-0002-5574-3165

Martin Böhning − *Bundesanstalt für Materialforschung und -prüfung (BAM), 12205 Berlin, Germany;* orcid.org/0000-0001-9753-345X

Bernhard Frick − *Institut Laue-Langevin, Grenoble 38000, France*

Markus Appel − *Institut Laue-Langevin, Grenoble 38000, France*

Richard A. Mole − *Australian Nuclear Science and Technology Organisation (ANSTO), Lucas Heights, NSW 2234, Australia*

Nicolas R. De Souza − *Australian Nuclear Science and Technology Organisation (ANSTO), Lucas Heights, NSW 2234, Australia;* orcid.org/0000-0003-4099-9544

Reiner Zorn − *Jülich Centre for Neutron Science (JCNS-1) and Institute for Biological Information Processing (IBI-8), Forschungszentrum Jülich GmbH, 52425 Jülich, Germany;* orcid.org/0000-0001-7321-8404

Complete contact information is available at: https://pubs.acs.org/10.1021/acs.macromol.4c01045

Notes

The authors declare no competing financial interest.

■ ACKNOWLEDGMENTS

We are grateful to Dr. Dmitry A. Alentiev and Dr. Maxim Bermeshev (Moscow) providing the Janus polynorbornenes to us. The Institut Laue-Langevin (ILL, Grenoble, France) and

the Australian Nuclear Science and Technology Organisation (ANSTO, Lucas Heights, Australia) are thanked for enabling the neutron scattering experiments (ANSTO proposal number 13420).

REFERENCES

(1) Baker, R. W. *Membrane Technology and Applications*; John Wiley & Sons: Chichester, UK, 2004.
(2) Yampolskii, Y. Polymeric gas separation membranes. *Macromolecules* **2012**, *45*, 3298−3311.
(3) Wijmans, J. G.; Baker, R. W. The solution-diffusion model: a review. *J. Membr. Sci.* **1995**, *107*, 1−21.
(4) Higashimura, T.; Masuda, T.; Okada, M. Gas Permeability of Polyacetylenes with Bulky Substituents. *Polym. Bull.* **1983**, *10*, 114−117.
(5) Masuda, T.; Kawasaki, M.; Okano, Y.; Higashimura, T. Polymerization of Methylpentynes by Transition Metal Catalysts: Monomer Structure, Reactivity, and Polymer Properties. *Polym. J.* **1982**, *14*, 371−377.
(6) Morisato, A.; Pinnau, I. Synthesis and Gas Permeation Properties of Poly(4-methyl-2-pentyne). *J. Membr. Sci.* **1996**, *121*, 243−250.
(7) Budd, P. M.; Msayib, K. J.; Tattershall, C. E.; Ghanem, B. S.; Reynolds, K. J.; McKeown, N. B.; Fritsch, D. Gas Separation Membranes from Polymers of Intrinsic Microporosity. *J. Membr. Sci.* **2005**, *251*, 263−269.
(8) Carta, M.; Malpass-Evans, R.; Croad, M.; Rogan, Y.; Jansen, J. C.; Bernardo, P.; Bazzarelli, F.; McKeown, N. B. An Efficient Polymer Molecular Sieve for Membrane Gas Separations. *Science* **2013**, *339*, 303−307.
(9) Wang, Y.; Ghanem, B. S.; Han, Y.; Pinnau, I. State-of-the-art polymers of intrinsic microporosity for high-performance gas separation membranes. *Curr. Opin. Chem. Eng.* **2022**, *35*, No. 100755.
(10) Swaidan, R.; Ghanem, B.; Litwiller, E.; Pinnau, I. Physical Aging, Plasticization and Their Effects on Gas Permeation in "Rigid" Polymers of Intrinsic Microporosity. *Macromolecules* **2015**, *48*, 6553−6561.
(11) Hofmann, D.; Heuchel, M.; Yampolskii, Y.; Khotimskii, V.; Shantarovich, V. Free Volume Distributions in Ultrahigh and Lower Free Volume Polymers: Comparison between Molecular Modeling and Positron Lifetime Studies. *Macromolecules* **2002**, *35*, 2129−2140.
(12) Heuchel, M.; Fritsch, D.; Budd, P. M.; McKeown, N. B.; Hofmann, D. Atomistic Packing Model and Free Volume Distribution of a Polymer with Intrinsic Microporosity (PIM-1). *J. Membr. Sci.* **2008**, *318*, 84−99.
(13) Chapala, P. P.; Bermeshev, M. V.; Starannikova, L. E.; Belov, N. A.; Ryzhikh, V. E.; Shantarovich, V. P.; Lakhtin, V. G.; Gavrilova, N. N.; Yampolskii, Y. P.; Finkelshtein, E. S. A Novel, Highly Gas-Permeable Polymer Representing a New Class of Silicon-Containing Polynorbornens as Efficient Membrane Materials. *Macromolecules* **2015**, *48*, 8055−8061.
(14) Gringolts, M.; Bermeshev, M.; Yampolskii, Y.; Starannikova, L.; Shantarovich, V.; Finkelshtein, E. New High Permeable Addition Poly(tricyclononenes) with $Si(CH_3)_3$ Side Groups. Synthesis, Gas Permeation Parameters, and Free Volume. *Macromolecules* **2010**, *43*, 7165−7172.
(15) Zotkin, M. A.; Alentiev, D. A.; Shorunov, S.; Sokolov, S. E.; Gavrilova, N. N.; Bermeshev, M. V. Microporous polynorbornenes bearing carbocyclic substituents. Structure-property study. *Polymer* **2023**, *269*, No. 125732.
(16) Alentiev, D. A.; Bermeshev, M. Design and synthesis of porous organic polymeric materials from norbornene derivatives. *Polym. Rev.* **2022**, *62*, 400−437.
(17) Guseva, M. A.; Alentiev, D. A.; Bakhtin, D. S.; Borisov, I. L.; Borisov, R. S.; Volkov, A. V.; Finkelshtein, E. S.; Bermeshev, M. V. Polymers based on exo-silicon-substituted norbornenes for membrane gas separation. *J. Membr. Sci.* **2021**, *638*, 119656.
(18) Wang, X.; Wilson, T. J.; Alentiev, D.; Gringolts, M.; Finkelshtein, E. S.; Bermeshev, M.; Long, B. K. Substituted polynorbornene membranes: a modular template for targeted gas separations. *Polym. Chem.* **2021**, *12*, 2947−2977.
(19) Fuoco, A.; Rizzuto, C.; Tocci, E.; Monteleone, M.; Esposito, E.; Budd, P. M.; Carta, M.; Comesañ-Gándara, B.; McKeown, N. B.; Jansen, J. C. The origin of size-selective gas transport through polymers of intrinsic microporosity. *J. Mater. Chem. A* **2019**, *7*, 20121−20126.
(20) Sundell, B. J.; Lawrence, J. A., III; Harrigan, D. J.; Vaughn, J. T.; Pilyugina, T. S.; Smith, D. R. Alkoxysilyl functionalized polynorbornenes with enhanced selectivity for heavy hydrocarbon separations. *RSC Adv.* **2016**, *6*, 51619−51628.
(21) Vaughn, J. T.; Harrigan, D. J.; Sundell, B. J.; Lawrence, J. A.; Yang, J. Reverse selective glassy polymers for C_{3+} hydrocarbon recovery from natural gas. *J. Membr. Sci.* **2017**, *522*, 68−76.
(22) Gmernicki, K. R.; Hong, E.; Maroon, C. R.; Mahurin, S. M.; Sokolov, A. P.; Saito, T.; Long, B. K. Accessing siloxane functionalized polynorbornenes via vinyl-addition polymerization for CO_2 separation membranes. *ACS Macro Lett.* **2016**, *5*, 879−883.
(23) Alentiev, D. A.; Egorova, E. S.; Bermeshev, M. V.; Starannikova, L. E.; Topchiy, M. A.; Asachenko, A. F.; Gribanov, P. S.; Nechaev, M. S.; Yampolskii, Y. P.; Finkelshtein, E. S. Janus Tricyclononene Polymers Bearing Tri(n-Alkoxy)Silyl Side Groups for Membrane Gas Separation. *J. Mater. Chem. A* **2018**, *6*, 19393−19408.
(24) Kolmangadi, M.; Szymoniak, P.; Smales, G. J.; Alentiev, D.; Bermeshev, M.; Böhning, M.; Schönhals, A. Molecular dynamics of Janus polynorbornenes: Glass transitions and nanophase separation. *Macromolecules* **2020**, *53*, 7410−7419.
(25) Beiner, M.; Huth, R. Nanophase separation and hindered glass transition in side-chain polymers. *Nat. Mater.* **2003**, *2*, 595−59.
(26) Inoue, R.; Kanaya, T.; Masuda, T.; Nishida, K.; Yamamuro, O. Relationship between the Local Dynamics and Gas Permeability of Para-Substituted Poly(1-chloro-2-phenylacetylenes). *Macromolecules* **2012**, *45*, 6008−6014.
(27) Kanaya, T.; Teraguchi, M.; Masuda, T.; Kaji, K. Local mobility of substituted polyacetylenes measured by quasielastic neutron scattering and its relationship with gas permeability. *Polymer* **1999**, *40*, 7157−7161.
(28) Kanaya, T.; Tsukushi, I.; Kaji, K.; Sakaguchi, T.; Kwak, G.; Masuda, T. Role of Local Dynamics in the Gas Permeability of Glassy Substituted Polyacetylenes. A Quasielastic Neutron Scattering Study. *Macromolecules* **2002**, *35*, 5559−5564.
(29) Böhning, M.; Hao, N.; Schönhals, A. Correlation of Activation Energies of Gas Diffusivity and Local Matrix Mobility in Polycarbonate/POSS Nanocomposites. *J. Polym. Sci. Polym. Phys.* **2013**, *51*, 1593−1597.
(30) Yin, H.; Chua, Y.; Yang, B.; Schick, C.; Harrison, W.; Budd, P. M.; Böhning, M.; Schönhals, A. First clear-cut experimental evidence of a glass transition in a polymer with intrinsic microporosity: PIM-1. *J. Chem. Phys. Lett.* **2018**, *9*, 2003−2008.
(31) Yin, H.; Yang, B.; Chua, Y. Z.; Szymoniak, P.; Carta, M.; Malpass-Evans, R.; McKeown, N. B.; Harrison, W. J.; Budd, P. M.; Schick, C.; Bohning, M.; Schonhals, A. Effect of Backbone Rigidity on the Glass Transition of Polymers of Intrinsic Microporosity Probed by Fast Scanning Calorimetry. *ACS Macro Lett.* **2019**, *8*, 1022−1028.
(32) Kolmangadi, M. A.; Szymoniak, P.; Zorn, R.; Böhning, M.; Wolf, M.; Zamponi, M.; Schönhals, A. Molecular mobility in high performance polynorbornenes: A combined broadband dielectric, advanced calorimetry, and neutron scattering investigations. *Polym. Eng. Sci.* **2022**, *62*, 2143−2155.
(33) Konnertz, N.; Ding, Y.; Harrison, W. J.; Budd, P. M.; Schönhals, A.; Bohning, M. Molecular mobility of the high performance membrane polymer PIM-1 as investigated by dielectric spectroscopy. *ACS Macro Lett.* **2016**, *5*, 528−532.
(34) Emamverdi, F.; Yin, H.; Smales, G. J.; Harrison, W. J.; Budd, P. M.; Böhning, M.; Schönhals, A. Polymers of Intrinsic Microporosity − Molecular Mobility and Physical Aging Revisited by Dielectric Spectroscopy and X-Ray Scattering. *Macromolecules* **2022**, *55*, 7340−7350.

https://doi.org/10.1021/acs.macromol.4c01045
Macromolecules 2024, 57, 8562−8575

(35) Yin, H.; Chapala, P.; Bermeshev, M.; Pauw, B. R.; Schönhals, A.; Böhning, M. Influence of trimethylsilyl side groups on the molecular mobility and charge transport in highly permeable glassy polynorbornenes. *ACS Appl. Polym. Mater.* **2019**, *1*, 844−855.
(36) Yin, H.; Chapala, P.; Bermeshev, M.; Schönhals, A.; Böhning, M. *ACS Macro Letter* **2017**, *6*, 813−818.
(37) Zorn, R.; Lohstroh, W.; Zamponi, M.; Harrison, W. J.; Budd, P.; Böhning, M.; Schönhals, A. Molecular mobility of a polymer of intrinsic microporosity revealed by quasielastic neutron scattering. *Macromolecules* **2020**, *53*, 6731−6739.
(38) Schonhals, A.; Szymoniak, P.; Kolmangadi, M. A.; Bohning, M.; Zamponi, M.; Frick, B.; Appel, M.; Gunther, G.; Russina, M.; Alentiev, D. A.; Bermeshev, M.; Zorn, R. Microscopic dynamics of highly permeable super glassy polynorbornenes revealed by neutron scattering. *J. Membr. Sci.* **2022**, *642*, No. 119972.
(39) Zorn, R.; Yin, H.; Lohstroh, W.; Harrison, W.; Budd, P. M.; Pauw, B. R.; Böhning, M.; Schönhals, A. Anomalies in the low frequency vibrational density of states for a polymer with intrinsic microporosity − the Boson peak of PIM-1. *Phys. Chem. Chem. Phys.* **2018**, *20*, 1355−1363.
(40) Zorn, R.; Szymoniak, P.; Kolmangadi, M.; Wolf, M.; Alentiev, D.; Bermeshev, M.; Böhning, M.; Schönhals, A. Low frequency vibrational density of state of highly permeable super glassy polynorbornenes − The Boson peak. *Phys. Chem. Chem. Phys.* **2020**, *22*, 18381.
(41) Szymoniak, P.; Kolmangadi, M. A.; Juranyi, F.; Bohning, M.; Zorn, R.; Schönhals, A. Low -frequency vibrational density of state of Janus-polynorbornenes: The dependence of the Boson peak on the nanophase-separated structure. *Macromolecules* **2023**, *56*, 5803−5812.
(42) Beiner, M.; Schröter, K.; Hempel, E.; Reissig, S.; Donth, E. Multiple glass transition and nanophase separation in poly(n-alkyl methacrylate) homopolymers. *Macromolecules* **1999**, *32*, 6278−6282.
(43) Warren, B. E. X-ray diffraction in long chain liquids. *Phys. Rev.* **1933**, *44*, 969.
(44) Yamamoto, T.; Komarudin, D.; Arai, M.; Lee, B.-L.; Suganuma, H.; Asakawa, N.; Inoue, Y.; Kubota, K.; Sasaki, S.; Fukuda, T.; Matsuda, H. Extensive studies on π-stacking of poly(3-alkylthiophene-2,5−2,5-diyl)a and poly(4-alkylthiazole-2,5-diyl) by optical spectroscopy NMR analysis, light scattering analysis, and X-ray crystallography. *J. Am. Chem. Soc.* **1998**, *120*, 2047−2058.
(45) Liberman-Martin, A. L.; Chang, A. B.; Chu, C. K.; Siddique, R. H.; Lee, B.; Grubbs, R. H. Processing effects on the self-assembly of bush block polymer photonic crystals. *ACS Macro Lett.* **2021**, *10*, 1480−1486.
(46) https://www.ill.eu/users/instruments/instruments-list/in16b/description/instrument-layout.
(47) Frick, B.; Mamontov, E.; Eijck, L. v.; Seydel, T. Rechent backscattering instrumentation developments at the ILL and SNS. *Zeitschrift für Physikalische Chemie* **2010**, *224*, 33−60.
(48) Schönhals, A.; Appel, M.; Frick, B.; Szymoniak, P.; Zorn, R. Incoherent neutron backscattering on Janus polynorbornenes. *Institut Laue-Langevin (ILL)* **2021**, DOI: 10.5291/ILL-DATA.6-04-287.
(49) Yu, D.; Mole, R.; Noakes, T.; Kennedy, S.; Robinson, R. Pelican − a time of flight cold neutron polarization analysis spectrometer at OPAL. *J. Phys. Soc. Jpn.* **2013**, *82*, SA027.
(50) Richard, D.; Ferrand, M.; Kearley, G. J. Analysis and Visualisation of Neutron-Scattering Data″. *J. Neutron Research* **1996**, *4*, 33−39.
(51) Arnold, O.; et al. Mantid — Data analysis and visualization package for neutron scattering and μSR experiments. *Nuclear Instruments and Methods in Physics Research Section A* **2014**, *764*, 156−166.
(52) Bée, M. *Quasielastic Neutron Scattering. Principles and Applications in Solid State Chemistry, Biology and Materials Science*; Adam Hilger: Bristol, UK, 1988.
(53) Zorn, R. On the evaluation of neutron scattering elastic scan data. *Nucl. Instr. Meth. A* **2009**, *603*, 439−445.
(54) Singwi, K. S.; Sjölander, A. Diffusive motion in water and cold neutron scattering. *Phys. Rev.* **1960**, *119*, 863.
(55) Schönhals, A.; Zorn, R.; Frick, B. Inelastic neutron scattering as a tool to investigate nanoconfined polymer systems. *Polymer* **2016**, *105*, 393−406.
(56) Schönhals, A.; Goering, H.; Schick, C.; Frick, B.; Zorn, R. Polymers in nanoconfinement: What can be learned from relaxation and scattering experiments. *J. Non-Cryst. Solids* **2005**, *351*, 2668−2677.
(57) Zorn, R. https://iffgit.fz-juelich.de/zorn/unift.
(58) Colmenero, J.; Moreno, A.; Alegria, A. *Prog. Polym. Sci.* **2005**, *30*, 1147−1184.
(59) Prager, M.; Heidemann, A. Rotational Tunneling and Neutron Spectroscopy: A Compilation. *Chem. Rev.* **1997**, *97*, 2933−2966.
(60) Zorn, R.; Frick, B.; Fetters, L. Quasielastic neutron scattering study of the methyl group dynamics in polyisoprene. *J. Chem. Phys.* **2002**, *116*, 845−853.
(61) Wuttke, J. Multiple-scattering effects on smooth neutron-scattering spectra. *Phys. Rev. E* **2000**, *62*, 6531.
(62) Zorn, R. Multiple scattering correction of polarized neutron diffraction data. *Nucl. Instr. Meth.* **2002**, *479*, 568−584.
(63) Yildirim, A.; Krause, C.; Zorn, R.; Lohstroh, W.; Schneider, G. J.; Zamponi, M.; Holderer, O.; Frick, B.; Schonhals, A. Complex molecular dynamics of a symmetric model discotic liquid crystal revealed by broadband dielectric, thermal and neutron spectroscopy. *Soft Matter* **2020**, *16*, 2005−2016.
(64) Arbe, A.; Colmenero, J.; Richter, D. Polymer dynamics by dielectric spectroscopy and neutron scattering. In *Broadband Dielectric Spectroscopy*; Kremer, F., Schönhals, A., Eds.; Springer: Berlin, 2003; pp 685−718.
(65) Kremer, F.; Schönhals, A. The scaling of the dynamics of glasses and supercooled liquids. In *Broadband dielectric spectroscopy*. Kremer, F., Schönhals, A., Eds.; Springer: Berlin, 2003; pp 99−130.
(66) Schönhals, A.; Kremer, F.; Schlosser, E. The scaling of the α-relaxation in low molecular glass forming liquids and polymers. *Phys. Rev. Lett.* **1991**, *67*, 999.
(67) Schönhals, A.; Schlosser, E. Dielectric relaxation in polymeric solids Part 1: A new model for the interpretation of the shape of the dielectric relaxation function. *Colloid Polym. Sci.* **1989**, *267*, 125.
(68) Colmenero, J.; Alegria, A.; Arbe, A.; Frick, B. Correlation between non-Debye and q-behavior of the alpha relaxation in glass-forming polymers. *Phys. Rev. Lett.* **1992**, *69*, 478−481.
(69) Colmenero, J; Arbe, A; Alegria, A; Monkenbusch, M; Richter, D On the origin of the non-exponential behavior of the alpha-relaxation in glass-forming polymers: Incoherent neutron scattering and dielectric relaxation results. *J. Phys.: Condens. Matter* **1999**, *11*, A363−A370.
(70) Alvarez, F.; Alegria, A.; Colmenero, J. Interconnection between frequency-domain Havriliak-Negami and time-domain Kohlrausch-Williams-Watts functions. *Phys. Rev. B* **1993**, *47*, 125−130.
(71) Tyagi, M.; Alegria, A.; Colmenero, J. Heterogeneous dynamics of poly(vinyl acetate) far above Tg: A combined study by dielectric spectroscopy and quasielastic neutron scattering. *J. Chem. Phys.* **2005**, *122* (2005), No. 244909.
(72) Arbe, A.; Colmenero, J.; Monkenbusch, M.; Richter, D. Dynamics of glass-forming polymers: "Homogeneous" versus Heterogeneous scenario. *Phys. Rev. Lett.* **1998**, *81*, 590.
(73) Vogel, H. The temperature dependence law of the viscosity of fluids. *Physikalische Zeitschrift* **1921**, *22*, 645−646.
(74) Fulcher, G. S. Analysis of recent measurements of the viscosity of glasses. *J. Am. Ceram. Soc.* **1925**, *8*, 339.
(75) Tammann, G.; Hesse, W. The dependence of viscosity on temperature in hypothermic liquids. *Zeitschrift für Anorganische und Allgemeine Chemie* **1926**, *156*, 245−257.
(76) Angell, C. A. Entropy and Fragility in Supercooling Liquids. *J. Res. Natl. Inst. Stand. Technol.* **1997**, *102*, 171−185.

https://doi.org/10.1021/acs.macromol.4c01045
Macromolecules 2024, 57, 8562−8575